Supplementary Information for
The 2023 Mw7.8 Kahramanmaraş, Turkey Earthquake: A Multi-segment Rupture in A Millennium Supercycle

Contents of this file

Tables S1. The coordinates of the aftershocks used to calibrate the BP results. The time and coordinates of the aftershocks from the AFAD catalog are shown on the left. The results of the aftershock locations before and after slowness calibration are shown along with their distance errors and root-mean-square error relative to the location in the AFAD catalog. (a) shows the results of the AK array BP of the Mw 7.8 event, (b) shows the results of the CH array BP of the Mw 7.8 event, (c) shows the results of the AK array BP of the Mw 7.5 event, and (d) shows the results of the CH array BP of the Mw 7.5 event.

(a)

AFAD			BP results (AK Mw 7.8)					
			Before calibration			After calibration		
time	longitude	latitude	longitude	latitude	Distance error (km)	longitude	latitude	Distance error (km)
2023-02-06T20:37:51	37.05	37.30	36.86	37.18	21.49	37.02	37.31	2.88
2023-02-07T03:13:12	37.66	37.81	37.59	37.55	29.51	37.63	37.75	7.16
2023-02-06T01:51:21	36.59	36.88	36.54	36.87	4.59	36.74	36.94	14.93
2023-02-06T05:36:32	36.14	36.34	35.90	36.26	23.31	36.06	36.34	7.18
2023-02-06T01:46:26	38.05	38.07	38.19	37.99	15.16	38.11	38.15	10.32
2023-02-06T02:03:36	37.88	37.91	37.95	37.71	23.04	37.91	37.87	5.16
2023-02-06T06:54:57	37.46	37.73	37.26	37.59	23.51	37.42	37.71	4.18
RMS error (km):					**21.42**			**8.32**

(b)

AFAD			BP results (CH Mw 7.8)					
			Before calibration			After calibration		
time	longitude	latitude	longitude	latitude	Distance error (km)	longitude	latitude	Distance error (km)
2023-02-06T20:37:51	37.05	37.30	37.1	37.19	12.99	37.1	37.31	4.57
2023-02-07T03:13:12	37.66	37.81	37.55	37.59	26.27	37.59	37.71	12.70
2023-02-06T10:51:28	38.19	38.31	38.07	38.19	16.96	38.19	38.32	1.11
2023-02-06T01:51:21	36.59	36.88	36.5	36.75	16.51	36.58	36.86	2.39
2023-02-06T16:32:11	36.39	36.70	36.42	36.62	9.27	36.41	36.74	4.79
2023-02-09T07:18:17	36.65	37.07	36.69	36.99	9.57	36.69	37.1	4.87
2023-02-06T02:01:45	36.99	37.29	36.9	37.19	13.67	36.94	37.27	4.96
2023-02-06T05:36:32	36.14	36.34	36.13	36.22	13.35	36.13	36.34	0.90
2023-02-06T04:16:49	37.26	37.50	37.22	37.35	17.02	37.27	37.47	3.45
2023-02-06T02:03:36	37.88	37.91	37.87	37.83	8.92	37.91	37.91	2.64
2023-02-06T06:54:57	37.46	37.73	37.43	37.55	20.15	37.47	37.67	6.72
RMS error (km):					**15.78**			**5.44**

(c)

AFAD			BP results (AK Mw 7.5)					
			Before calibration			After calibration		
time	longitude	latitude	longitude	latitude	Distance error (km)	longitude	latitude	Distance error (km)
2023-02-06T12:02:11	36.48	38.07	36.65	38.07	14.92	36.49	38.07	0.88
2023-02-06T21:57:43	36.54	38.06	36.69	38.03	13.58	36.53	38.07	1.41
2023-02-06T17:26:24	36.59	38.12	36.73	38.1	12.48	36.61	38.11	2.08
2023-02-08T14:20:25	37.39	37.99	37.46	37.95	7.59	37.42	37.99	2.64
2023-02-06T13:44:49	37.57	38.01	37.66	37.99	8.21	37.62	37.99	4.92
RMS error (km):					**11.73**			**2.77**

(d)

AFAD			BP results (CH Mw 7.5)					
			Before calibration			After calibration		
time	longitude	latitude	longitude	latitude	Distance error (km)	longitude	latitude	Distance error (km)
2023-02-06T12:02:11	36.48	38.07	36.37	38.07	9.65	36.49	38.07	0.88
2023-02-06T21:57:43	36.54	38.06	36.41	38.03	11.89	36.53	38.07	1.41
2023-02-06T17:26:24	36.59	38.12	36.41	38.07	16.74	36.53	38.11	5.38
2023-02-06T21:15:17	37.07	38.06	36.98	38.03	8.57	37.06	38.07	1.41
2023-02-08T14:20:25	37.39	37.99	37.3	37.94	9.66	37.38	37.95	4.53
2023-02-06T13:44:49	37.57	38.01	37.5	38.02	6.25	37.54	38.03	3.44
RMS error (km):					**10.96**			**3.32**

Table S2. The information of the M5.3 aftershock used for Mach wave search.

Time (UTC)	Latitude	Longitude	Magnitude (Mw)
2023-02-06 20:37:51	37.2588° N	37.1017° E	5.3

Table S3. A summary of fault parameters on the four segments of EAF. Long-term slip rates are from Duman and Emre (2013). Lengths (L) are determined based on our FFI fault plane lengths and fault maps in Duman and Emre (2013). Rigidity and G-R law constants are from Güvercin et al. (2022). The seismogenic depth is determined according to our coseismic model and the seismicity distribution in Güvercin et al. (2022).

Fault Segment	Pütürge	Erkenek	Pazarcık	Amanos
Long-term fault slip rates (mm/yr)	10	7	7	3
Length (L, km)	96	60	121	131
a value in G-R law	4.5	3.2	3.9	3.8
b value in G-R law	0.96	0.88	0.94	0.92
Corresponding FFI fault planes (Figure 1b)	East part of S3	West part of S3	S2, S4, East part of S5	S6, west part of S5
Rigidity (μ, GPa)	35			

Seismogenic depth (H, km)	20

Table S4. The significant historical events included in the moment history calculation (Ambraseys & Jackson, 1998; Palutoglu & Sasmaz, 2017).

Time	Longitude	Latitude	Magnitude	Reference
601	36.5	37.0	/	Ambraseys & Jackson, 1998
1114	37.5	37.5	7.8	Ambraseys & Jackson, 1998
1795	37.3	37.6	7	Palutoglu & Sasmaz, 2017
1822	36.5	36.7	7.5	Ambraseys & Jackson, 1998
1872	36.4	36.4	7.2	Ambraseys & Jackson, 1998
1874	39.5	38.5	7.1	Ambraseys & Jackson, 1998
1875	39.5	38.5	6.7	Ambraseys & Jackson, 1998
1893	38.3	38.0	7.1	Ambraseys & Jackson, 1998
1905	38.6	38.1	6.8	Ambraseys & Jackson, 1998
2020	39.09	38.5	6.7	Chen et al., 2020

Table S5. Synthetic Aperture Radar (SAR) pairs analyzed.

Sensor	Pass / Track	Preseismic Date	Postseismic Date	Acquisition Time [UTC]
S1A	Asc / 14	2023-01-28	2023-02-09	15:34
S1A	Dsc / 21	2023-01-29	2023-02-10	03:34

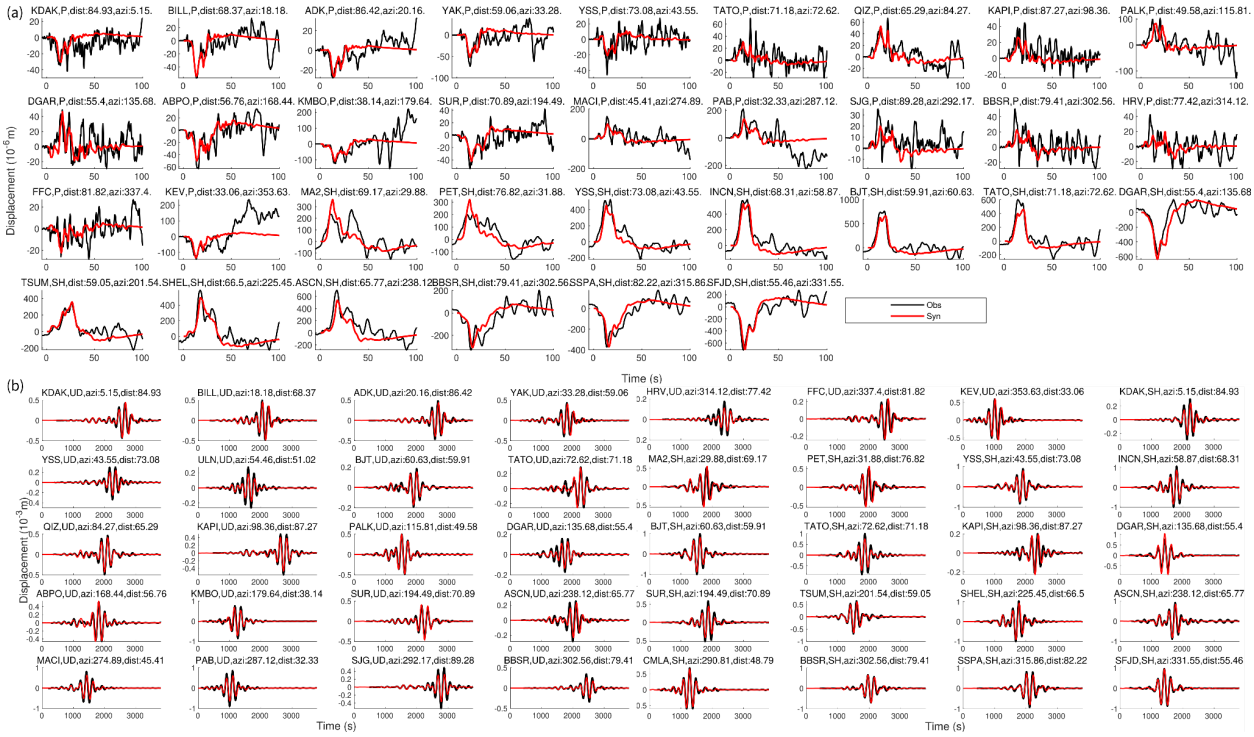

Extended Data Figure 1. Comparison between observed teleseismic wave waveforms (black lines) and synthetic seismograms (red lines) generated by the preferred model of the Mw 7.8 event. (a) The broadband P and S waves. (b) The long-period surface waves. The wave type and the station name are shown at the top of each trace, along with azimuth and epicenter distance in degree.

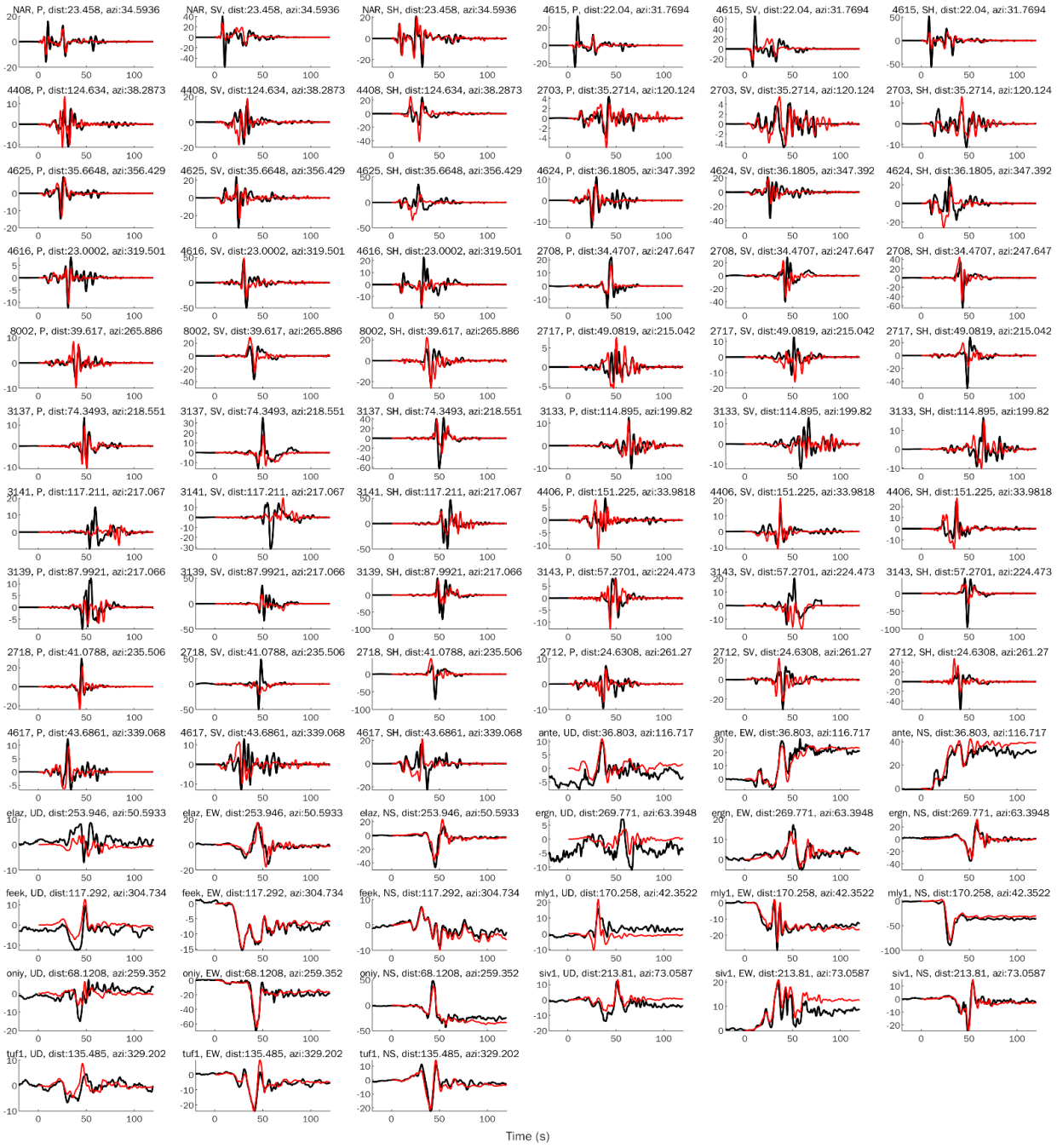

Extended Data Figure 2. Comparison between observed near-field strong motion station or high-rate GNSS waveforms (black lines) and synthetic seismograms (red lines). The component and the station name are shown at the top of each trace, accompanied by azimuth and epicenter distance in km. Subplots 1-57 (stations NAR to 4617) are strong motion recordings, with the unit of cm/s. Subplots 58-81 (stations ante to tuf1) are high-rate GNSS recordings, with the unit of cm.

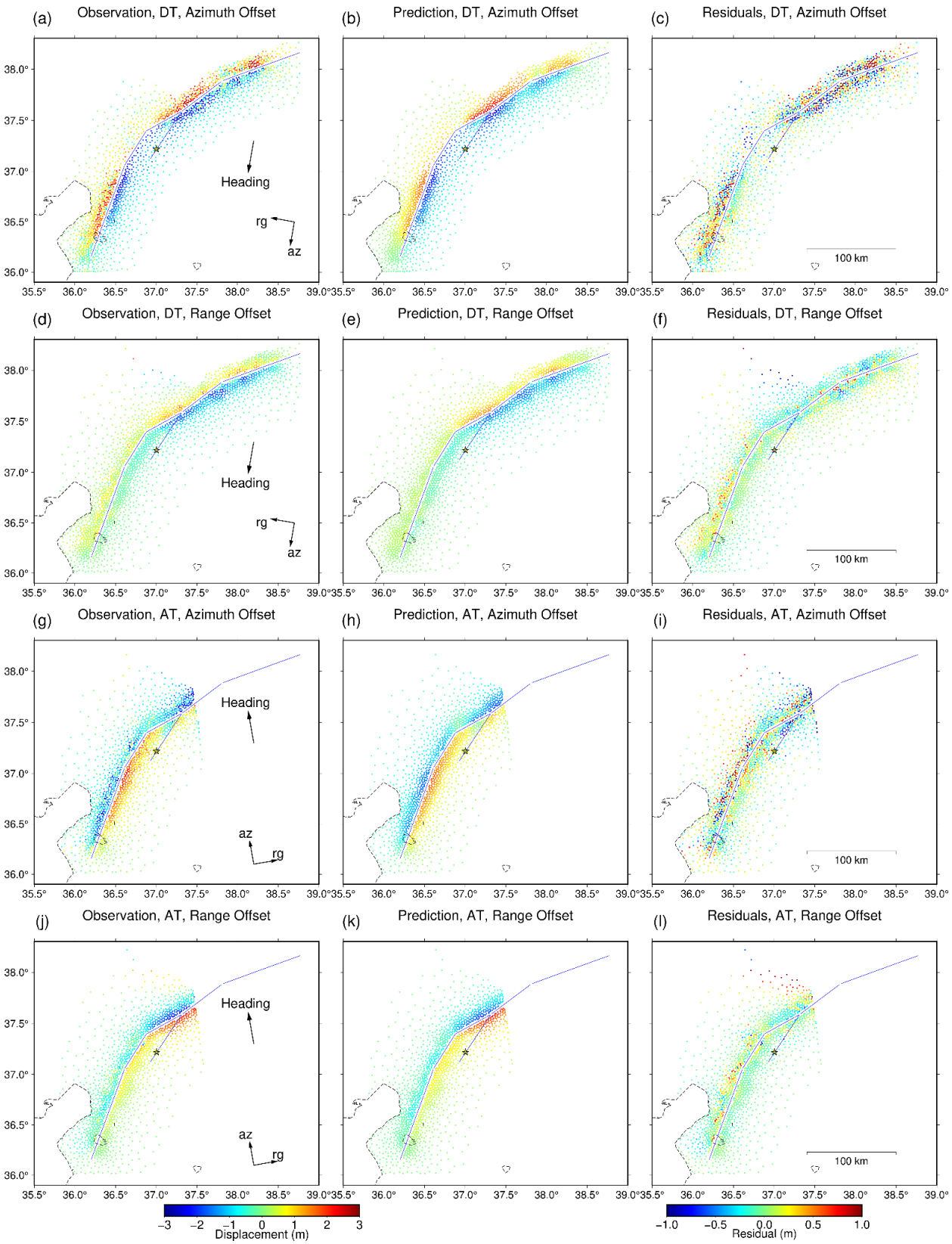

Extended Data Figure 3. The sub-sampled static displacement data fits. The first column is the resampled static displacement (observation). The second column is the prediction by the

preferred model. The third column is the residuals obtained by deducting the prediction from the observation.

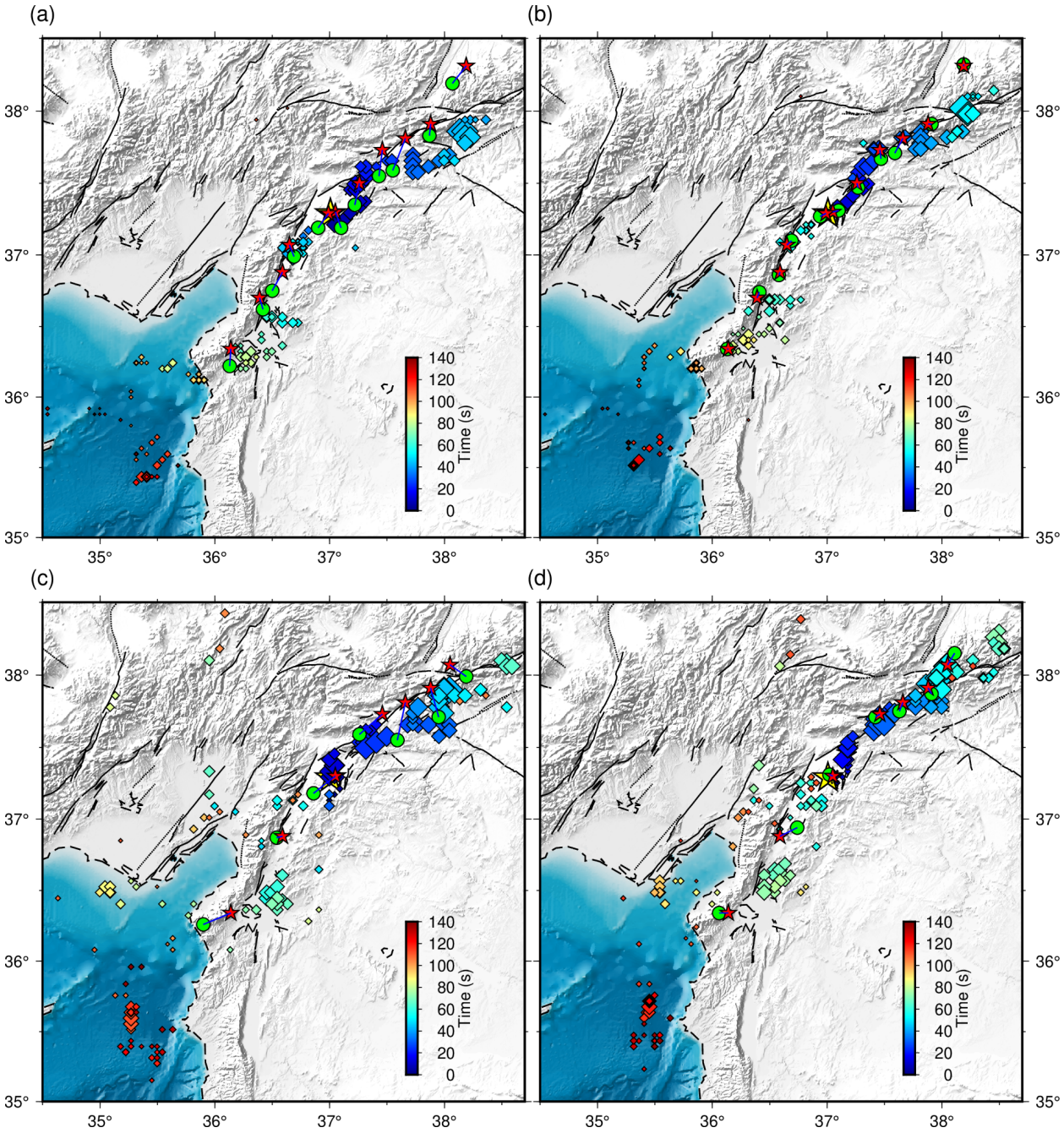

Extended Data Figure 4. Comparison of aftershock locations and mainshock BPs (the Mw 7.8 event) before and after calibration. (a) The CH array's results before slowness calibration. (b) The CH array's results after slowness calibration. (c) The AK array's results before slowness calibration. (d) The AK array's results after slowness calibration. Green circles denote the BP-inferred locations of M 4.7+ aftershocks spanning the rupture region. The red stars denote the AFAD catalog of aftershocks. The yellow star denotes the epicenter of the mainshock. Diamonds denote the High-Freq radiators for the Mw 7.8 event, color-coded by rupture time relative to the origin time of the event and with a size proportional to the normalized BP power.

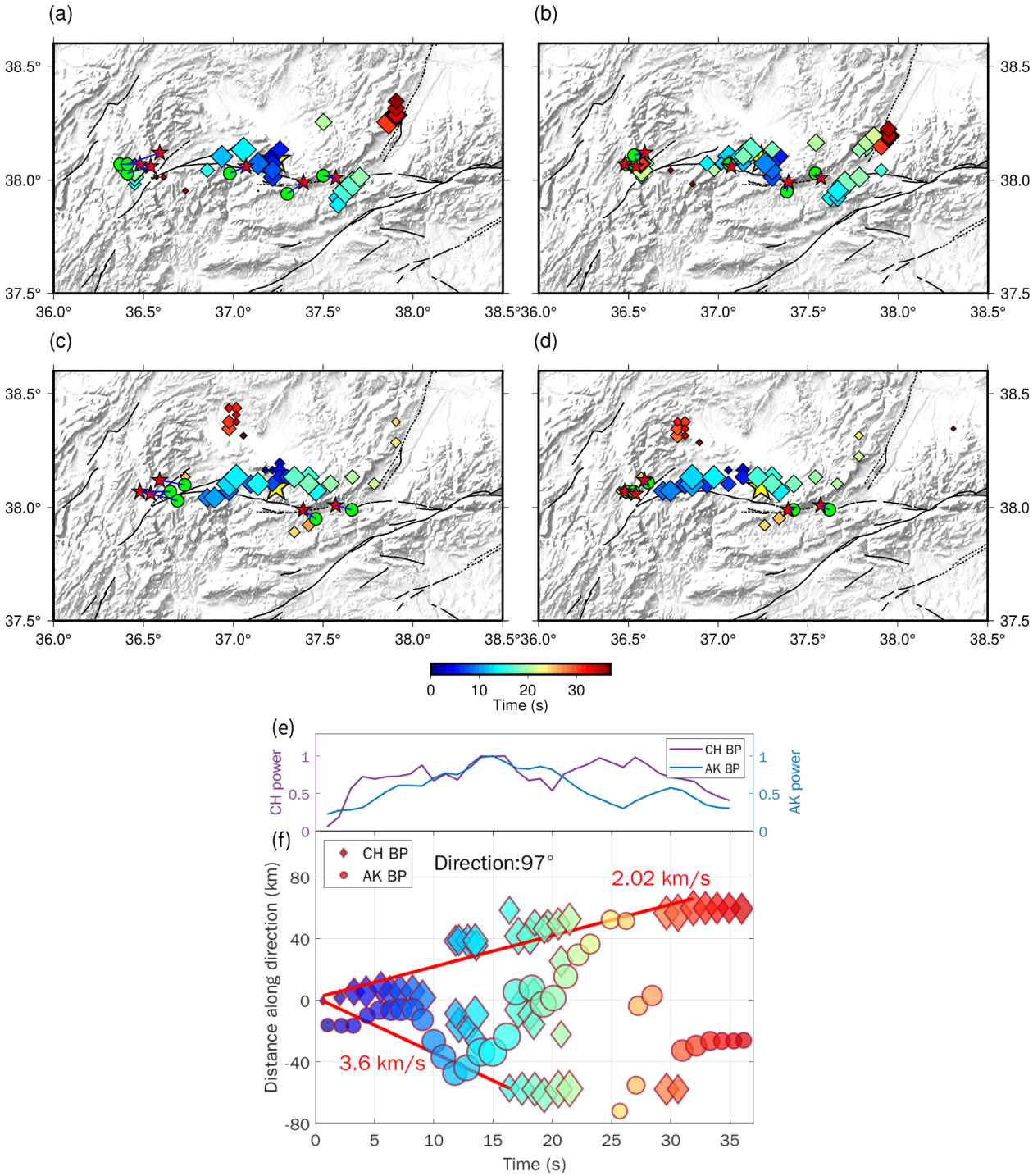

Extended Data Figure 5. Comparison of aftershock locations and mainshock BPs (the Mw 7.5 event) before and after calibration. (a) The CH array's results before slowness calibration. (b) The CH array's results after slowness calibration. (c) The AK array's results before slowness calibration. (d) The AK array's results after slowness calibration. Green circles denote the BP-inferred locations of M 4.7+ aftershocks spanning the rupture region. The red stars denote the AFAD catalog of aftershocks. The yellow star denotes the epicenter of the mainshock. Diamonds

denote the High-Freq radiators for the Mw 7.5 event, color-coded by rupture time relative to the origin time of the event and with a size proportional to the normalized BP power. (e) The BP power. The blue and purple curves denote the normalized BP power of AK and CH arrays, respectively. (f) The rupture speeds. The circles denote the High-Freq radiators imaged by the AK array, color-coded by rupture time relative to the origin time of the event and with a size proportional to the normalized BP power. The diamonds denote the same as circles but imaged by the CH array. The red slants and numbers show the fitted rupture speeds for the east branch (97°, positive direction) and for the west branch (277°, negative direction).

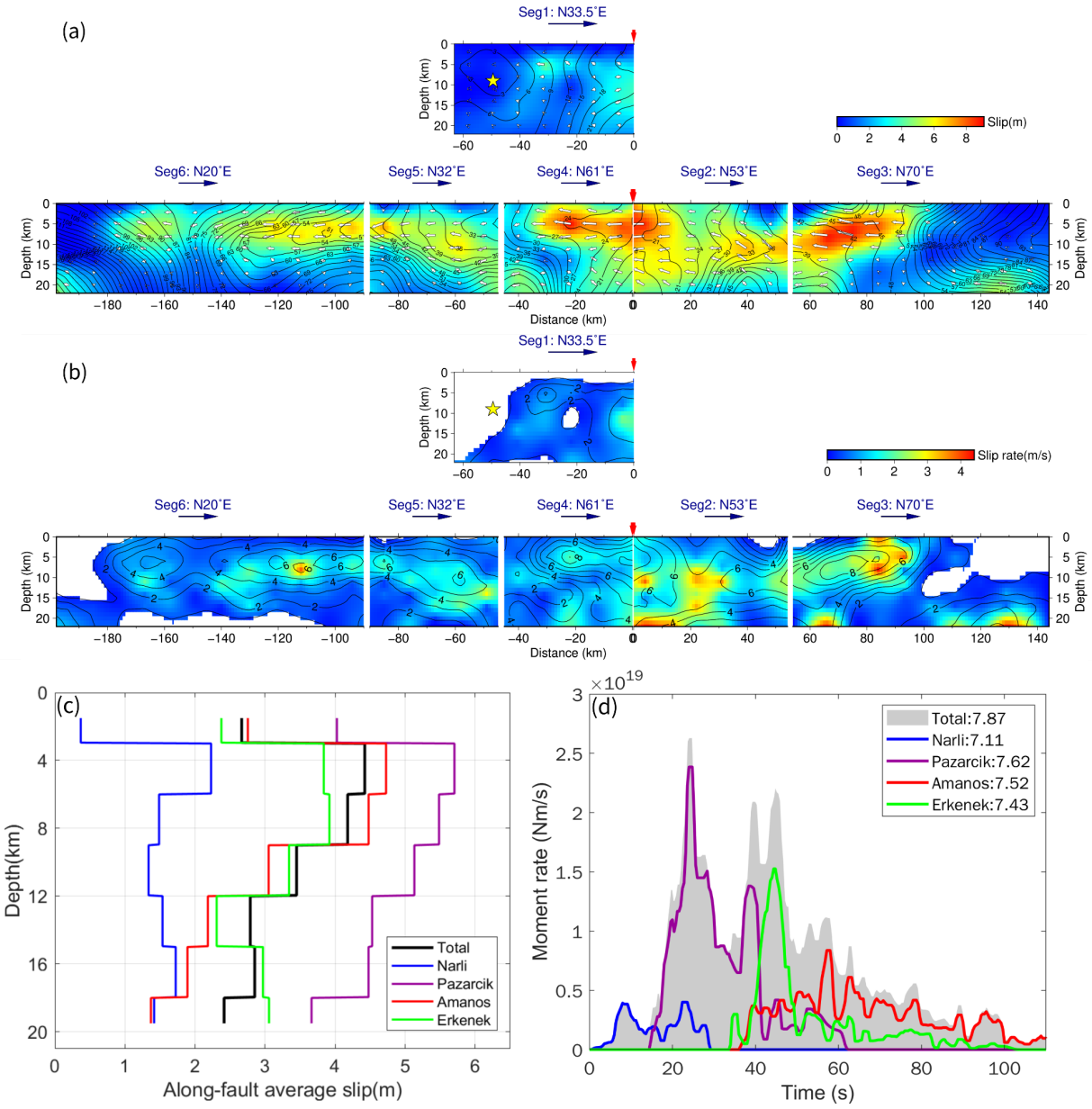

Extended Data Figure 6. The preferred slip model of the Mw 7.8 event. (a) The cross-section view of the slip distribution. The segment index and orientation are shown on the top of each segment. The red arrows indicate the connecting edges of S1, S2, and S4 segments. The black contours denote the slip initiation time. (b) The average slip rate defined as the slip amplitude (in meter) over rise time (in second). The black contours denote the slip of the preferred model (in meter). Only sub-sources with slip >= 10% maximum slip are displayed since the rise time for minor slip subfaults is often poorly constrained[9]. (c) The along-fault averaged slip as a function of depth for all fault segments and the entire slip model. (d) Moment rate functions. The gray-shaded area represents the whole rupture process. The color lines indicate the moment rate function on each fault segment. The moment magnitude on each segment is shown in the legend.

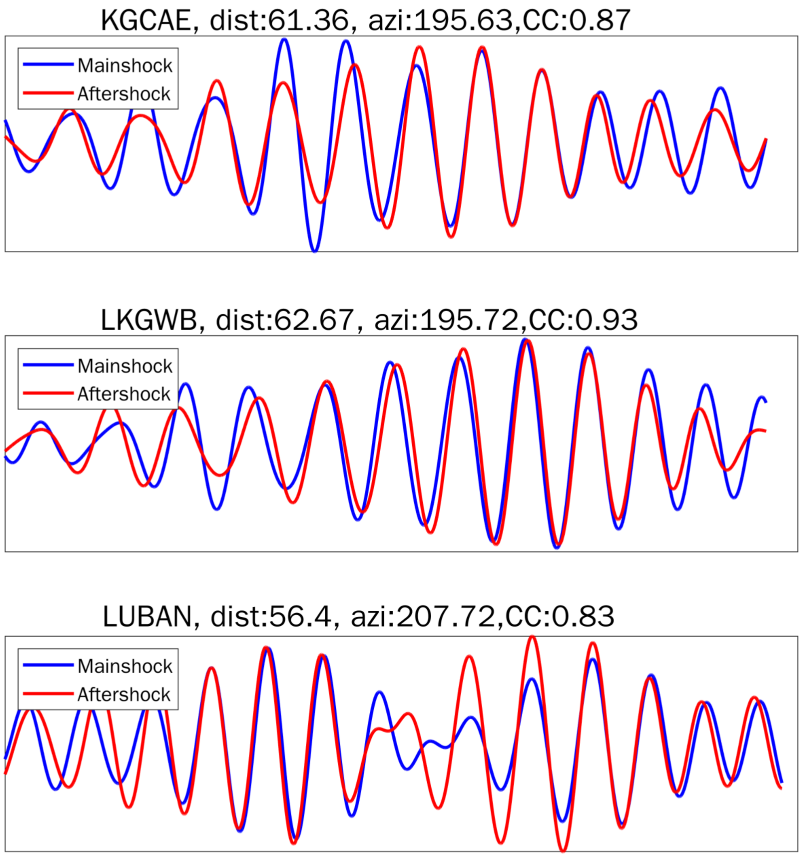

Extended Data Figure 7. The Rayleigh wave vertical displacement seismograms of mainshock (blue) and aftershock (red) in the 15–25 s period range recorded at stations located in the direction of south rupture. Station name, azimuths (azi), hypocentral distance (dist), and correlation coefficient (CC) are shown in the titles.

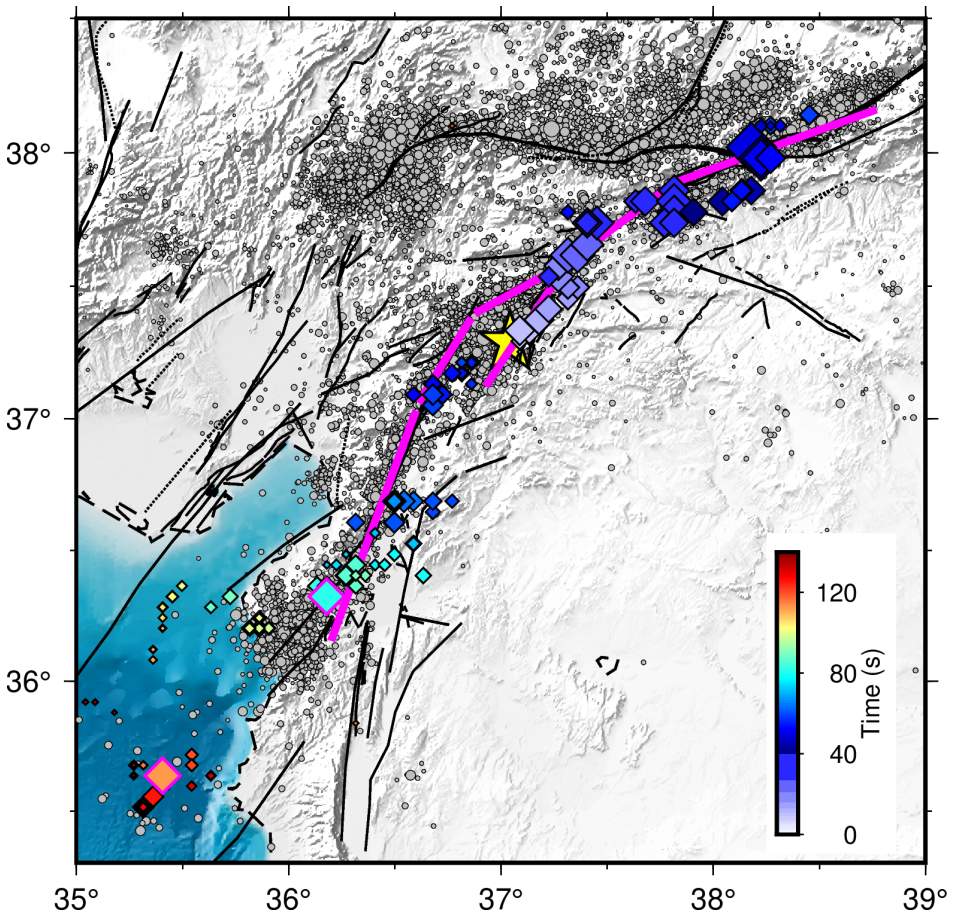

Extended Data Figure 8. Two High-Freq radiators used for S wave travel time calculation. The cyan diamond with magenta edge is the last radiator on the Amanos segment, and the red diamond with magenta edge is the first radiator for the triggered offshore event.

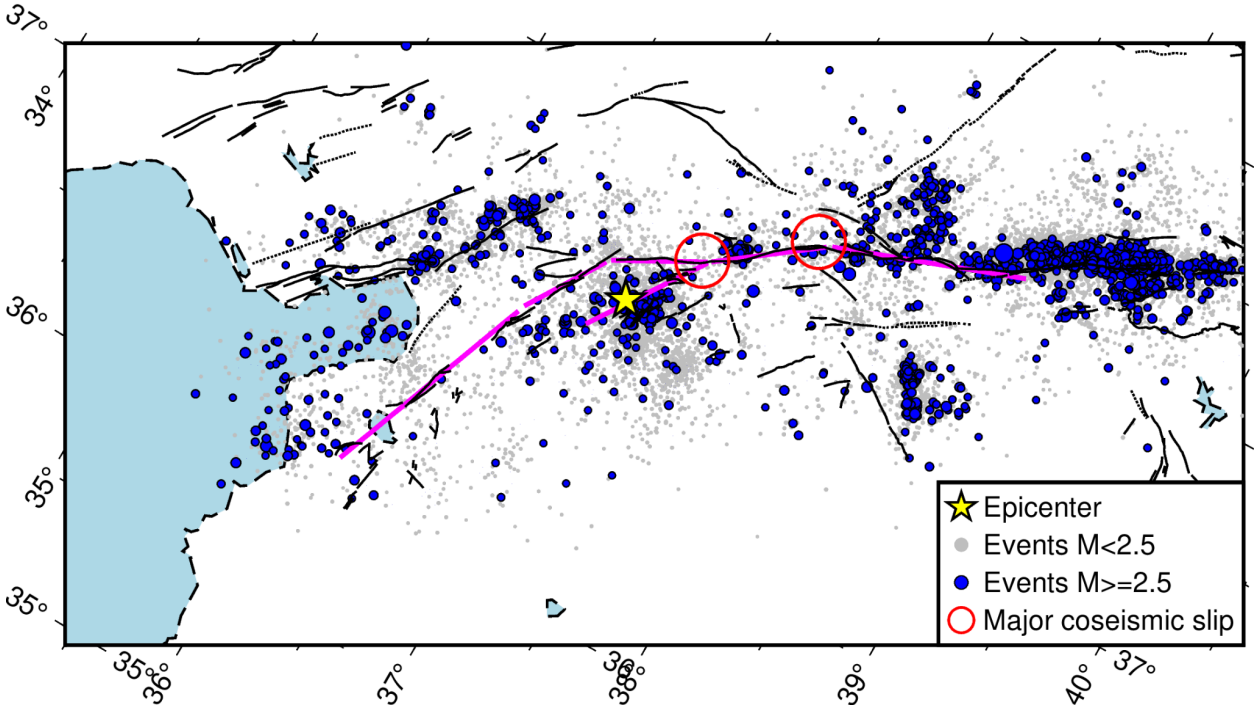

Extended Data Figure 9. Consistency between seismicity voids and major coseismic slip asperities. The red circles highlight the regions where large coseismic slip and seismicity voids appear simultaneously. The seismicities occurred between 2007 to 2020 and are from Güvercin et al.[2].

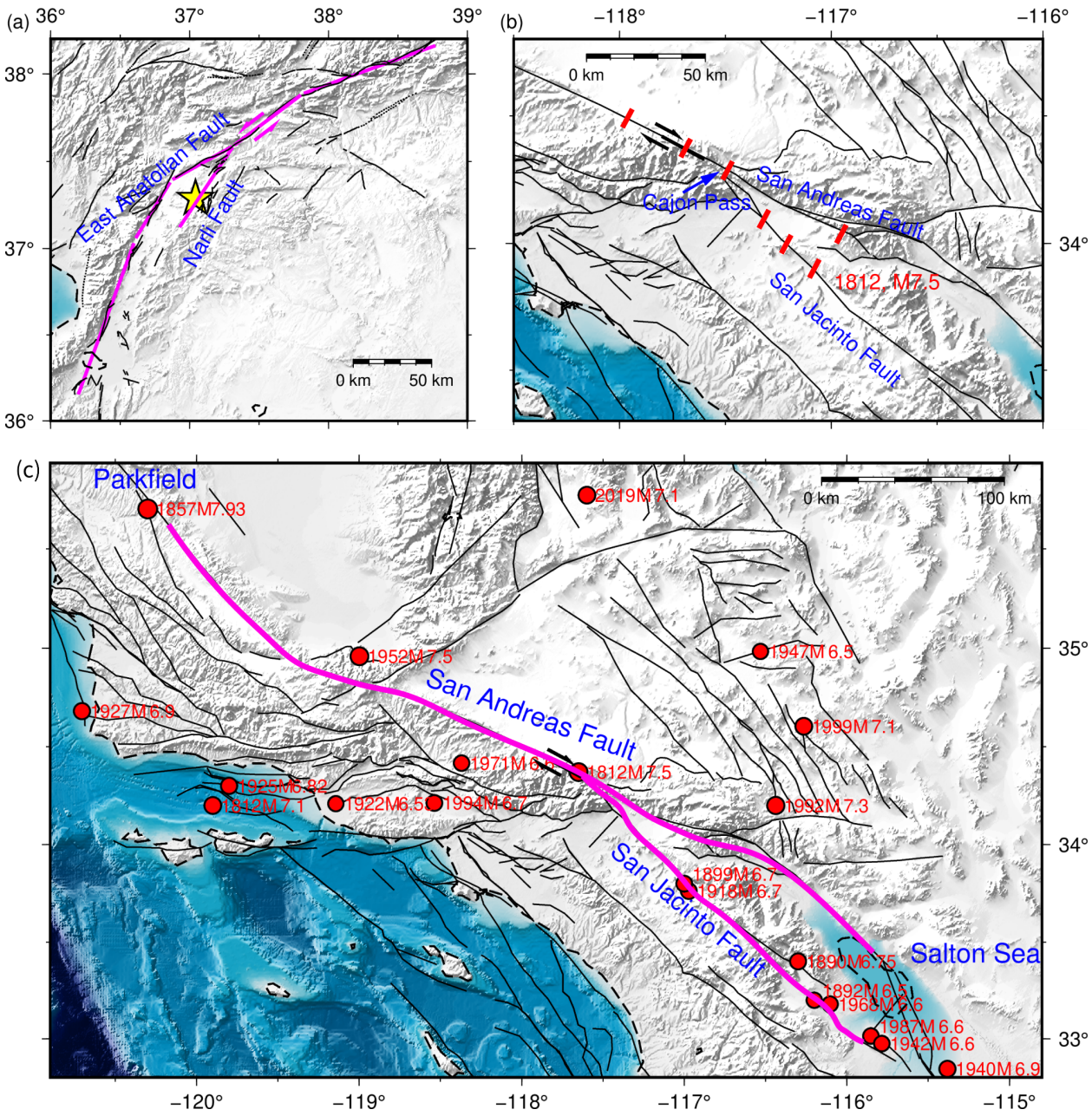

Extended Data Figure 10. Map of the East Anatolian Fault and San Andreas Fault systems. The magenta arrows in (a) and black arrows in (b) show fault motions. The yellow star in (a) denotes the epicenter of the 2023 Mw7.8 event. Red bars in (b) represent the paleoseismic sites of the early 1800 earthquake, adapted from Lozos[45]. (c) Historical earthquakes on and near San Andreas Fault and San Jacinto Fault since 1800. Earthquake locations and magnitudes are from USGS ANSS catalog. The magenta curve highlights the SAF and SJF segments that have not occurred by M>7 events since 1857.

Captions for Movies S1-S5:

Movie S1. The snapshot showing the rupture propagation of the Mw 7.8 event resolved by joint FFI. The white diamonds and circles denote the High-Freq radiators resolved by SEBP of CH array and AK array, respectively.

Movie S2. The rupture process of the Mw 7.8 event resolved by SEBP using CH array. The red asterisk denotes the hypocenter of the mainshock. The white star denotes the hypocenter of the Mw 6.7 aftershock occurring ~11 minutes later. The white lines denote the fault traces. The magenta points denote the aftershocks occurring between Jan 1, 2023 to Feb 8, 2023.

Movie S3. The rupture process of the Mw 7.8 event resolved by SEBP using the AK array. The red asterisk denotes the hypocenter of the mainshock. The white star denotes the hypocenter of the Mw 6.7 aftershock occurring ~11 minutes later. The white lines denote the fault traces. The magenta points denote the aftershocks occurring between Jan 1, 2023 to Feb 8, 2023.

Movie S4. The rupture process of the Mw 7.5 event resolved by SEBP using the CH array. The red asterisk denotes the hypocenter of the mainshock. The white lines denote the fault traces. The magenta points denote the aftershocks occurring between Jan 1, 2023 to Feb 8, 2023.

Movie S5. The rupture process of the Mw 7.5 event resolved by SEBP using the AK array. The red asterisk denotes the hypocenter of the mainshock. The white lines denote the fault traces. The magenta points denote the aftershocks occurring between Jan 1, 2023 to Feb 8, 2023.

References of Supplement Information:

Ambraseys, N. Temporary seismic quiescence: SE Turkey, *Geophys. J. Int.* **96**, 2, 311–331 (1989)

Ambraseys, N. & Jackson, J. Faulting associated with historical and recent earthquakes in the Eastern Mediterranean region, *Geophys. J. Int.* **133**, 2, 390–406 (1998).

Duman T.Y. & Emre Ö. The East Anatolian Fault: geometry, segmentation and jog characteristics, *Geol. Soc. Spec. Publ.*, **372**, 495–529 (2013).

Güvercin, S. E., Karabulut, H., Konca, A. Ö., Doğan, U., & Ergintav, S. Active seismotectonics of the East Anatolian Fault. *Geophys. J. Int.* **230**, 1, 50–69 (2022).

Palutoglt. M., Sasmaz. A. 29 November 1795 Kahramanmaras Earthquake, Southern Turkey. *Bulletin of the Mineral Research and Exploration*. **155**, 155, 187 - 202 (2017).